Phonon-mediated tunneling into a two-dimensional electron gas on the Be(0001) surface

Hermann Osterhage,* Roland Wiesendanger, and Stefan Krause
Department of Physics, University of Hamburg, Jungiusstrasse 11, 20355 Hamburg, Germany

(Received 7 October 2020; revised 31 March 2021; accepted 6 April 2021; published 27 April 2021)

The electronic properties of the Be(0001) surface are investigated on the atomic scale at low temperature. Utilizing laterally resolved scanning tunneling spectroscopy (STS) a pronounced surface state is identified, additionally manifested by the observation of bias-dependent standing-wave patterns. Fourier analysis reveals a parabolic dispersive behavior, being characteristic for a two-dimensional free-electron gas confined to the Be(0001) surface. Moreover, signatures of the opening of inelastic phonon-mediated tunnel channels for electrons near the Fermi level are observed by STS.

DOI: 10.1103/PhysRevB.103.155428

I. INTRODUCTION

Beryllium is a very unique element among the metals. Whereas an isolated Be atom has a very simple closed-shell $1s^2 2s^2$ electron configuration, interatomic bonding in Be crystals is realized by the hybridization between s and p bands [1–3]. At the Be(0001) surface the atomic coordination number is reduced, resulting in an anomalously large outward expansion [3]. Moreover, in the bulk Be behaves almost like a semiconductor, since the density of states (DOS) at the Fermi level E_F is very low [4,5]. In contrast, the Be(0001) surface is much more metallic [6–8], with an almost free-electron DOS that is originating from electronic surface states [5,8–11] that are strongly localized within the first two atomic planes [12]. Consequently, the Be(0001) surface is considered to be an ideal model system to host a two-dimensional electron gas with pronounced electron-electron and electron-phonon interactions that are decoupled from the bulk [13].

Scanning tunneling microscopy (STM) and spectroscopy (STS) are powerful tools to investigate electron systems on surfaces with precision down to the atomic scale [14–16]. In a first STM study on the Be(0001) surface, a pronounced pattern of electron standing waves has been observed [17]. The wave amplitude for energies near E_F was found to be anomalously large and interpreted as an indication for many-body effects like a charge density wave (CDW) or an enhanced electron-phonon coupling of the lattice. This hypothesis stimulated further studies on the Be(0001) surface. The electron-phonon coupling in this surface was indeed found to be large [7,18–20] and attributed primarily to surface-state electrons [20,21]. However, photoemission experiments did not confirm a gap in the DOS at E_F associated with a CDW [22,23]. Consequently, the origin of the standing-wave pattern on the Be(0001) surface remained an open question.

In our study, we revisit the Be(0001) surface utilizing laterally resolved STS at low temperatures. The surface state onset is identified in broad range spectroscopy, and standing-wave patterns are observed in maps of the differential conductance taken in the vicinity of atomic step edges or defect sites. Systematically analyzing these patterns by Fourier analysis as a function of tunnel bias reveals the detailed structure of the surface state, yielding a parabolic dispersive behavior between the surface state onset and E_F. This finding is characteristic for an almost free two-dimensional electron gas confined to the surface [24]. From the data, the effective mass of the electrons is extracted, being in good agreement with previous experimental studies. Detailed tunneling spectroscopy reveals a partial reduction of the differential conductance located symmetrically around E_F. It is attributed to the closing of electron tunnel channels as soon as inelastic electron-phonon scattering processes are forbidden due to the laws of energy and momentum conservation.

II. EXPERIMENTAL SETUP AND SAMPLE PREPARATION

All experiments were performed under ultrahigh vacuum conditions at pressures below 2×10^{-10} mbar, using home-built STM setups for studies at $T = 4.2$ K [25] and variable T, respectively. The differential tunneling conductance dI/dU was measured using a lock-in technique with ac modulation voltages of $U_{mod} \leqslant 40$ mV rms and a frequency of $f = 4815$ Hz applied to the tunnel junction in addition to a dc bias voltage U. Measurements were carried out using chemically etched Cr and W tips. The Be crystals were mechanically polished *ex situ* [26] and cleaned *in situ* by cycles of room temperature Ar^+ sputtering at pressures $p < 2 \times 10^{-5}$ mbar with energies of 1–2 keV and annealing at temperatures of up to 800 °C. After several hours of sputtering and annealing, this procedure removed the oxide layers on the Be surface [27], but contaminations from the bulk of the crystal are promoted to the surface during the annealing. In a subsequent step, the surface was depleted from impurities by 3–4 h of soft Ar^+ sputtering (300 eV) at 580 °C and $p < 5 \times 10^{-6}$ mbar.

III. SCANNING TUNNELING MICROSCOPY

A constant current STM image of a Be(0001) surface resulting from this cleaning procedure is shown in Fig. 1(a). Atomically flat terraces are observed that are separated by

*hosterha@physnet.uni-hamburg.de

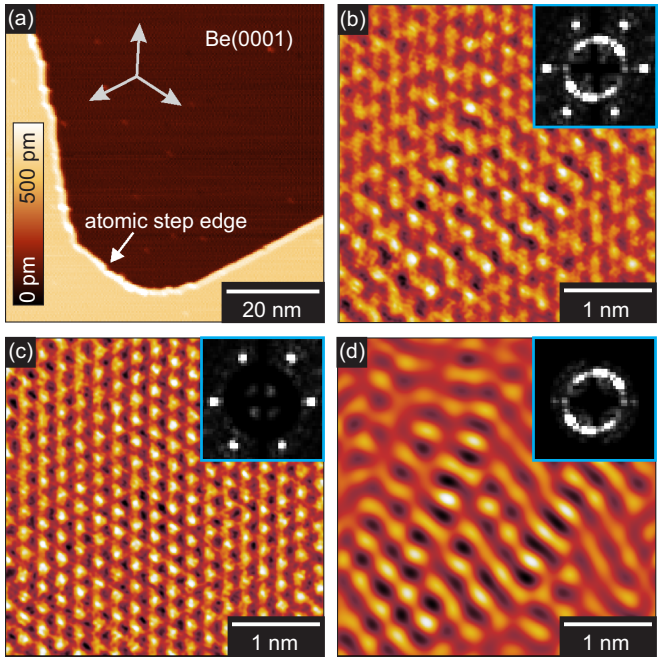

FIG. 1. Constant current STM images of the Be(0001) surface. (a) Atomically flat terraces are separated by an atomic step edge. High-symmetry directions of the crystal are indicated with arrows ($T = 4.2$ K, $I = 100$ pA, $U = 1.4$ V). (b) High-resolution STM image and its Fourier spectrum (inset). (c) The transformation of the spot features reveals the atomic lattice, whereas (d) the ring feature of the Fourier spectrum corresponds to standing waves ($T = 60$ K, $I = 10$ nA, $U = 10$ mV).

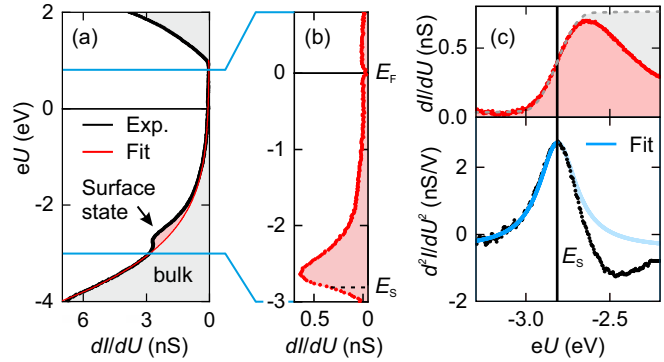

FIG. 2. Scanning tunneling spectroscopy on Be(0001). (a) Typical tunneling spectroscopy curve. A shoulder indicates the onset of the surface state (arrow). Bulk contributions are separated from the surface state by fitting with a polynomial (red line) ($T = 4.2$ K). (b) Surface-state contribution extracted from the spectrum in (a). (c) Top: Higher resolution spectroscopy around the surface state onset (red). A symmetric conductance step is sketched in gray. Bottom: numerical derivative d^2I/dU^2. The peak position determines the onset energy E_s, and fitting the rising flank with a Lorentzian peak (blue) results in the lifetime Γ_s.

atomic step edges preferentially running along the high-symmetry directions. In Fig. 1(b), a high-resolution STM image is shown, acquired with U corresponding to electrons tunneling with energies E close to E_F. Its Fourier spectrum is shown in the inset. It reveals six individual spots and a ring. A selective back-transformation of the six spots into real-space results in a very regular pattern that corresponds to the atomic lattice of the Be(0001) surface, as shown in Fig. 1(c). Transforming the ring into real-space results in the pronounced standing-wave pattern shown in Fig. 1(d). Its period of (3.4 ± 0.1) Å agrees well with the findings of previous STM studies on this surface [17]. Consequently, the STM image shown in Fig. 1(b) is a convolution of the atomic lattice and the electronic standing-wave texture on the Be(0001) surface, and selective Fourier filtering allows for their clear separation.

IV. ELECTRONIC STRUCTURE

For a detailed understanding of the electronic structure on the Be(0001) surface we performed tunneling spectroscopy by recording dI/dU as a function of electron energy eU with the tip positioned stationary at constant tip height. An exemplary spectrum covering a broad range of eU is shown in Fig. 2(a). Here the probe tip is stabilized at $U = -4$ V and $I = 7.75$ nA. The spectroscopy curve exhibits a very asymmetric shape with respect to E_F, which is a consequence of the unique electronic structure of Be: Between E_F and 1 eV, a plateau of a low dI/dU signal is observed. It reflects the semimetallic nature of Be, caused by a broad partial bulk band gap around E_F [11,21]. Above 1 eV, a steep rise in the dI/dU signal is found, which we assign to the DOS onset of the bulk conduction band [11,21,28]. When approaching E_F for $E < E_F$, a general trend of a decreasing dI/dU signal is found. It is known that the bulk DOS of Be drastically decreases when approaching E_F from below [21]. Simultaneously, the momentum parallel to the surface $k_\parallel$ increases when approaching E_F, resulting in a decrease of the tunneling probability between the tip and the sample [29]. Consequently, the spectroscopy curve below E_F can be interpreted as predominantly resulting from electrons tunneling elastically from Be bulk states.

On closer inspection a shoulder feature is found on top of this general curve, as indicated by the arrow in Fig. 2(a). As has been shown in previous STS studies on noble metal surfaces, an additional conductance channel opens when eU exceeds a value corresponding to the onset energy E_s of a surface-state band. It contributes to the tunneling process, leading to a steplike increase of the dI/dU signal [30–32]. Likewise, we attribute the shoulder feature to the onset of the Be(0001) surface state. Fitting the bulk contribution with a fourth-order polynomial background and subtracting it from the spectrum results in an approximation of the surface-state contribution shown in Fig. 2(b).

In the top panel of Fig. 2(c), the surface-state contribution to the dI/dU signal is plotted around E_s in more detail. Obviously, the step feature is significantly broadened, which is a consequence of finite lifetime effects [24]. For a model-type two-dimensional surface state, a constant DOS is expected that results in a plateau in the signal for energies above E_s, as indicated by the dotted line in Fig. 2(c). However, the signal decreases, which is in accordance with the observation of surface states by STS on metallic systems [32,33]: The geometry of the STM leads to preferential tunneling of electrons with

momentum perpendicular to the sample surface. Due to the increasing in-plane momentum $k_\parallel$ of the surface state with increasing energy, the tunneling conductance is suppressed, resulting in the decreasing signal.

In the bottom panel of Fig. 2(c), the numerical derivative d^2I/dU^2 is shown. The peak position corresponds to the surface state onset, and fitting with a local parabolic yields $E_s = (-2.81 \pm 0.01)$ eV, which is in good agreement with previous experiments and density functional theory [10,11,19,34].

The linewidth Γ_s of the surface state can be extracted as the width of the peak. Fitting the data with a Lorentzian profile of the form

$$\frac{d^2I}{dU^2}(U) \propto \frac{\Gamma_s}{4(eU - E_s)^2 + \Gamma_s^2} \tag{1}$$

yields a width of $\Gamma_s = (272 \pm 4)$ meV when restricting to the rising flank up to $eU = E_s$. Our value is roughly in accordance with the low-temperature value of $\Gamma_s \approx 350$ meV extrapolated from angle-resolved photoemission spectroscopy (ARPES) data [19]. Note the lateral averaging nature of photoemission experiments, while we restrict our study to high-purity surface areas, which potentially results in different values for Γ_s.

V. SURFACE-STATE DISPERSION

Figure 3(a) shows an exemplary series of dI/dU maps taken of the same surface area in the vicinity of an atomic step edge, imaged at three different bias voltages. Evidently, a variation of U between -1800 and $+200$ mV drastically changes the period of the pattern. This finding clearly indicates a dispersive behavior of the standing waves on the Be(0001) surface. In Fig. 3(b) a straight atomic step edge is shown that separates adjacent Be terraces. The step edges are found to preferentially run along directions of high symmetry, thereby acting as well-defined one-dimensional scattering centers for electrons and generating pronounced standing-wave patterns that fade away with distance from the step edge.

Utilizing the scanning probe capabilities of STM, we performed a laterally resolved study of the standing-wave pattern by recording tunneling spectra as a function of distance from an individual Be(0001) atomic step edge. At each setpoint x of the step edge distance, the tip is vertically positioned at the respective stabilization parameters with closed feedback loop. Subsequently the feedback loop is opened, and dI/dU spectra were recorded by ramping U between -3.0 and $+0.7$ V. This procedure results in the spectroscopy map shown in Fig. 3(c). It resolves the standing-wave pattern along the $[10\bar{1}0]$ direction as a function of electron energy eU.

A clear change in the wave periodicity with eU is visible, which reflects the dispersive behavior of the Be(0001) surface state. In order to extract the detailed dispersion relation, each horizontal line in Fig. 3(c) is analyzed in reciprocal space, utilizing one-dimensional fast Fourier transformation along x. Note that the wave number of standing electron waves seen in STM corresponds to twice the wave number k of the involved electronic states [14,16]. The resulting absolute values of the Fourier components in the $\bar{\Gamma}$-$\bar{M}$ direction are shown in the color plot in Fig. 3(d). Here, the horizontal axis corresponds

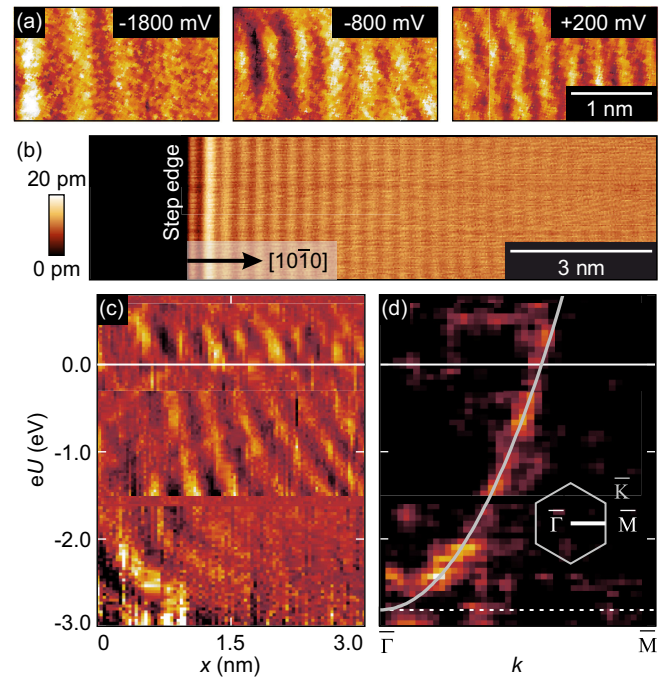

FIG. 3. Laterally resolved scanning tunneling spectroscopy on Be(0001). (a) Bias-dependent dI/dU maps, acquired at values of U as indicated. The periodic length clearly changes with U ($T = 4.2$ K, $I = 8, 5, 3$ nA). (b) Constant current STM image of standing waves emanating from a step edge that runs along a high-symmetry direction ($T = 4.2$ K, $I = 1$ nA, $U = -100$ mV). The propagation direction of standing electron waves is along $[10\bar{1}0]$. (c) Color plot of tunneling spectra taken as a function of distance x from an atomic step edge. Bias ranges: $[-3.0; -1.6]$ V; $[-1.5; -0.3]$ V; $[-0.3; 0.7]$ V. Stabilization conditions: (-3.0 V, 2 nA); (-1.5 V, 2 nA); (-0.3 V, 1 nA). Each horizontal row is normalized to its mean value. (d) Normalized Fourier components along the $\bar{\Gamma}$-$\bar{M}$ direction calculated from (c). A parabolic dispersion of the surface state is observed (solid line).

to k in the first Brillouin zone. From the spectral weights of the Fourier components a parabolic behavior is clearly deduced. It indicates a free-electron-like dispersive behavior of the two-dimensional electron gas in the surface state on Be(0001), in agreement with previous laterally averaging photoemission experiments [10]. The dispersion of a two-dimensional electron gas can generally be described by

$$E(k_\parallel) = \frac{\hbar^2 k_\parallel^2}{2m^*} + E_s. \tag{2}$$

Using E_s from above, the effective electron mass m^* can be extracted. For this, the sum of the spectral weights along supposed parabolic dispersion curves given by Eq. (2) is calculated as a function of m^*. Best accordance between the experimental data and the model is achieved for $m^* = (1.16 \pm 0.01)m_e$, with m_e being the free-electron mass. The respective dispersion is plotted on top of the color map in Fig. 3(d). Our finding is in good agreement with previous photoemission studies that found values between $1.19m_e$ and $1.27m_e$ [22,35].

In conclusion, the standing-wave pattern observed on the Be(0001) surface can be fully described within the concept

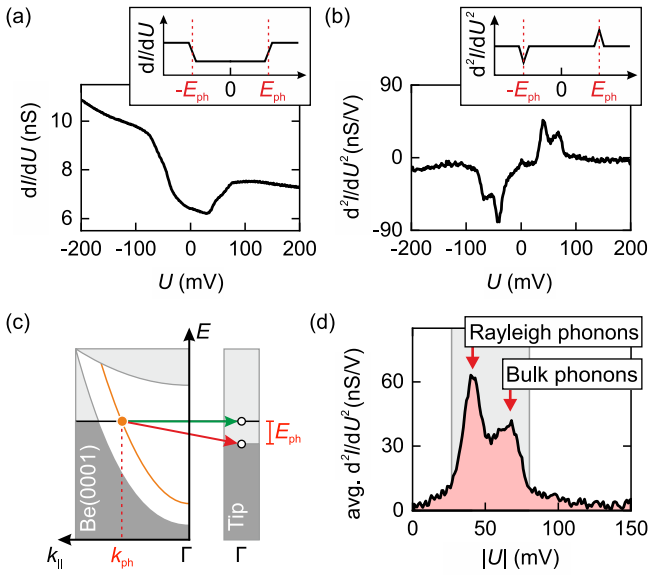

FIG. 4. (a) STS of Be(0001), measured with a W tip ($T = 4.2$ K, $U_{\text{stab}} = -200$ mV, $I_{\text{stab}} = 1.83$ nA, $U_{\text{mod}} = 2$ mV RMS) and (b) its numerical differentiation d^2I/dU^2. The insets schematically depict signatures of inelastic excitations. (c) Schematic representation of the elastic (green) and inelastic (red) tunneling processes involving surface-state electrons (orange) originating from Be(0001). Filled (empty) bulk bands are indicated in dark (light) gray. (d) Averaged d^2I/dU^2 signal over the positive and negative bias absolute values in (b). Arrows mark the peaks at 41 and 67 mV, respectively. The region of sizable inelastic excitations is marked in gray.

of a surface state, with electrons scattering at atomic-scale defects such as step edges or impurity atoms.

VI. PHONON-ASSISTED TUNNELING

On closer inspection of the data shown in Fig. 2(b), a dip is observed in dI/dU around E_F. To elaborate the details of this feature, we performed a high-resolution tunneling spectroscopy study as shown in Fig. 4(a). A double-step feature is clearly visible, together with an overall background signal that monotonously decreases with increasing U. It is well known from previous STM studies that steplike features located symmetrically around $U = 0$ indicate the opening of additional tunneling channels that are connected to inelastic excitations, as, for example, phonon excitations. As soon as the energy of a tunneling electron is high enough to generate a phonon with a certain threshold energy E_{ph}, this inelastic tunneling channel becomes available, on top of the elastic tunneling, thereby increasing dI/dU, as schematically depicted in the inset of Fig. 4(a) [36,37]. Numerically calculating the derivative of the signal allows for the precise determination of the excitation energies as peak positions in d^2I/dU^2. The respective curve is shown in Fig. 4(b). An almost point-symmetric curve is observed, with two dips for $U < 0$ and two peaks for $U > 0$. They are located at $eU = \pm 41$ meV and $eU = \pm 67$ meV, respectively.

We infer from our spectroscopy study that electron-phonon coupling is of high relevance for electron tunneling. Note that $k_\parallel$ for electrons in the Be(0001) surface state near E_F is considerably large, resulting in a suppression of elastic tunneling [36]. However, when the energy of the tunneling electron exceeds the energy of a phonon mode with matching momentum, an inelastic tunnel channel opens. For $U < 0$, electrons tunnel from the Be(0001) surface state to the tip, and the electron momentum is transferred to the Be lattice via the generation of phonons with momentum $k_{\text{ph}} = k_\parallel$. For $U > 0$, the situation is reversed, and electrons originating from the Γ point at the tip tunnel into the Be(0001) surface state with finite $k_\parallel$. Here, conservation of momentum is realized by the generation of phonons with $k_{\text{ph}} = -k_\parallel$. In previous studies the Rayleigh phonon mode was found to exhibit a dispersion with energies up to approximately 41 meV for the largest wave vector [7,21,38]. It is known from previous studies that Rayleigh phonons on the Be(0001) surface couple strongly to the electronic surface states [7,21,38]. Interestingly, pronounced peaks are observed at ± 41 meV in Fig. 4(b). We attribute this finding to the onset of the Rayleigh phonon generation, opening a channel for phonon-assisted tunneling across the vacuum barrier as depicted in Fig. 4(c). It adds to the elastic channel with electrons effectively tunneling between the sample and the tip, with the emitted phonon conserving energy and momentum [39,40]. Likewise, we attribute the peak at 67 meV to the opening of an additional channel for inelastic tunneling via coupling to a different phonon mode. With eU approaching E_s, $k_\parallel(eU)$ reduces, thereby increasing the differential tunneling conductance of the elastic channel. Simultaneously, the electron-phonon coupling is markedly weaker at E_s compared to E_F [7], hence the inelastic tunneling contribution decreases towards E_s. At E_s, phonon-mediated tunneling is suppressed and the tunnel current is dominated by elastic electron tunneling from the surface to the STM probe tip. Consequently, the ratio between elastic and inelastic tunneling changes significantly with U.

The electron-phonon coupling as a function of energy is described by the Eliashberg function α^2F, representing the phonon DOS weighed by the interaction strength [7]. This function has been derived for the Be(0001) surface at E_F using density functional theory [7] and ARPES [20,41]. As d^2I/dU^2 is proportional to α^2F [36,42], our STS data can be interpreted as a measure of the electron-phonon coupling. The choice of W as a tip material with weak electron-phonon coupling minimizes the influence of the tip on the inelastic tunneling spectrum [43]. The average of d^2I/dU^2 over positive and negative values of U is depicted in Fig. 4(d). The bias range of considerable inelastic contributions to the tunnel spectrum [gray area in Fig. 4(d)] corresponds to the energy range of high DOS in the phonon spectrum of Be(0001) [1]. The two peaks in Fig. 4(d) indicate energies where the electron-phonon coupling is significantly enhanced. The peak at 41 meV, associated with the Rayleigh mode localized in the Be(0001) surface, is well distinguished in our data. It agrees with α^2F derived from density functional theory [7], as well as ARPES results for the $\overline{\Gamma}$-$\overline{M}$ direction [41]. The second peak is located at 67 meV, where bulk phonons contribute primarily to α^2F [20], and was similarly observed in ARPES [20,41]. Thus the symmetric step around E_F seen in the spectrum in Fig. 4(a) is not a signature of decreased electronic DOS. It can be attributed to a reduced tunneling probability near

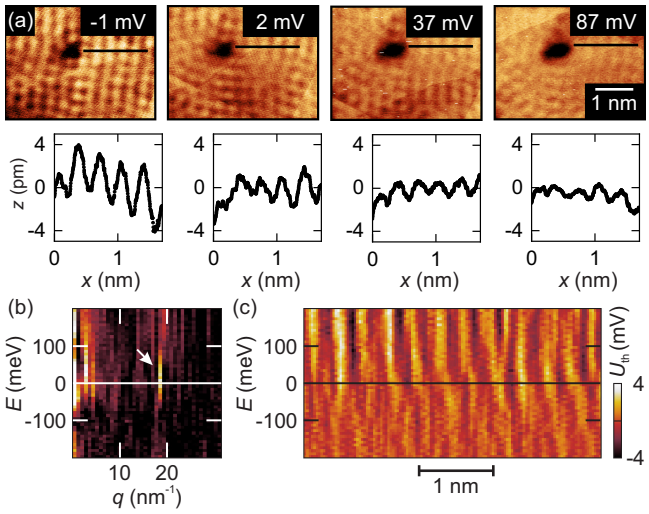

FIG. 5. (a) Constant-current STM images of the standing-wave pattern acquired at different bias voltages as indicated ($I = 1$ nA; $T = 40$ K). Cross sections taken along the lines in the images indicate respective typical wave amplitudes, ranging between 1 and 4 pm. (b) Detailed view of the FFT-STS obtained around E_F. A pronounced spectral weight of the standing wave is observed within the energy window of maximum phonon energies (arrow). (c) Thermovoltage U_{th}, as derived from the laterally resolved spectroscopy data and projected to a situation where the sample and the tip are at a temperature of 150 and 300 K, respectively. A significant variation of U_{th} is found on the standing-wave pattern.

E_F compared to inelastically enhanced tunneling for higher electron energies.

VII. COMPARISON WITH PREVIOUS STUDIES

In our STS study, we investigated the standing-wave pattern within a wide energy window, ranging from the surface state onset at -2.81 eV up to $+0.700$ eV with respect to the Fermi energy. Analyzing the standing-wave pattern amplitude, we observed a general tendency to decrease with increasing absolute bias, as shown in Fig. 5(a). One reason for this is the stronger damping of the oscillations due to increasing electron-electron interaction for energies away from E_F [44]. Moreover, the larger bulk contribution to the total tunnel conductance for high negative bias values results in a diminishing surface-state contribution to the measured signal, thereby effectively decreasing the observed wave amplitude. The wave pattern observed in our experiments exhibits a corrugation between 2 and 4 pm, even for energies in very close vicinity of the Fermi energy. It roughly increases by a factor of 2 between -1 and 37 mV bias, determined from the line profiles in Fig. 5(a).

In Fig. 5(b), the dispersion around E_F is shown in detail. Here, the dI/dU signal is normalized to its mean value before calculating the weights of the Fourier components. The dispersion of the wave pattern is again observed, with pronounced spectral weights within an energy window of $\approx$80 meV around E_F. This window corresponds to the range of phonon energies on Be(0001). Such pronounced spectral weights have been observed before by STM studies on metallic systems [45]. It is a consequence of the closing of the scattering channel at energies below the threshold for phonon generation, resulting in longer-lived quasiparticles near E_F and a higher DOS due to renormalization of the quasiparticle dispersion.

In previous STM studies on Be(0001), a standing-wave amplitude variation by a factor of ten was observed between -2.1 and -35 mV, with the highest corrugation of up to 42 pm near E_F. Such a drastic enhancement was never observed in our experiments. We speculate that the previously observed amplitude enhancement stems from a significant contribution of thermal Seebeck tunneling to the overall tunnel current: Whereas the sample was held at a temperature of 150 K, the tip remained at room temperature [46]. It is known that a temperature difference across the tunnel junction adds a laterally varying thermovoltage to the tunnel bias in STM experiments [47]. Consequently, a huge thermal gradient is present between the tip and the sample, resulting in a thermovoltage that potentially exceeds the fixed external bias voltage. This effect alters the observed amplitude of standing electron waves, especially for small bias values. While scanning across the wave pattern on the Be(0001) surface, local electronic variations in terms of density of states and its first derivative result in a significant variation of the thermovoltage between the tip and the sample [48].

In our work the tip and the sample were in thermal equilibrium, and hence no thermovoltage is expected. Analyzing spectroscopy data taken in almost perfect thermal equilibrium allows one to predict values for the thermovoltage [49]. From our spectroscopy data taken on the wave pattern on Be(0001) at $T = 4.2$ K we roughly estimate the thermovoltage for a situation where the sample is at 150 K and the tip is held at room temperature (300 K). Based on our data we infer a thermovoltage $U_{th}(\vec{r})$ that varies between approximately ± 2 mV for low bias setpoints, depending on the tip being located above the wave maxima or minima on Be(0001), as shown in Fig. 5(c). The STM image with the most enhanced wave pattern amplitude in Ref. [17] was taken at a bias setpoint of $U = -2$ mV. Including thermovoltage effects from our projected STS results, the contribution of Seebeck tunneling under these experimental conditions results in an effective bias $U_{eff} = U + U_{th}(\vec{r})$ between the tip and the standing-wave pattern on the sample that ranges between $U = -4$ mV and $U = 0$ mV. We expect this change of effective bias having severe consequences for the constant-current imaging of the Be(0001) surface, eventually resulting in ill-defined tunneling conditions that yield very enhanced amplitudes of the wave pattern around E_F. As shown in Fig. 5(c), the Seebeck tunneling effect becomes less significant with increasing bias setpoint and can be neglected for negative biases that are more than 20 mV away from the Fermi level.

VIII. CONCLUSIONS

We have performed a detailed STS study to elaborate the details of electron tunneling into the Be(0001) surface state. Electronic standing-wave patterns on the surface are identified as Friedel oscillations of the free-electron-like surface state. The strong electron-phonon interaction at the Be(0001) surface that spurred speculations about a possible formation

of a CDW is reflected in a sizable inelastic contribution to the tunneling current. However, no indications for the presence of a CDW were found. Moreover, no drastic enhancement of oscillation amplitudes within a few meV around E_F was found. Our study reveals that the electronic and phononic properties of the Be(0001) surface are distinct from the bulk properties. The Be(0001) surface is found to host a two-dimensional electron gas, being strongly coupled to surface phonon modes. Together with its simple electronic configuration, the Be(0001) surface represents an almost ideal model system for theoretical as well as experimental studies, shedding light on the details of fundamental electron-electron and electron-phonon interactions in low dimensions.

ACKNOWLEDGMENTS

We thank V. Přikryl, R. Dao, and K. Oetker for their assistance in the experimental work and M. Wenderoth for scientific discussions. Financial support from the Deutsche Forschungsgemeinschaft (DFG) via Grant No. KR3771/2-1 is gratefully acknowledged.

[1] J. B. Hannon, E. J. Mele, and E. W. Plummer, Phys. Rev. B **53**, 2090 (1996).
[2] P. J. Feibelman, Phys. Rev. B **46**, 2532 (1992).
[3] H. L. Davis, J. B. Hannon, K. B. Ray, and E. W. Plummer, Phys. Rev. Lett. **68**, 2632 (1992).
[4] I. Vobornik, J. Fujii, M. Hochstrasser, D. Krizmancic, C. E. Viol, G. Panaccione, S. Fabris, S. Baroni, and G. Rossi, Phys. Rev. Lett. **99**, 166403 (2007).
[5] E. W. Plummer and J. B. Hannon, Prog. Surf. Sci. **46**, 149 (1994).
[6] P. Hofmann, B. G. Briner, M. Doering, H.-P. Rust, E. W. Plummer, and A. M. Bradshaw, Phys. Rev. Lett. **79**, 265 (1997).
[7] A. Eiguren, S. de Gironcoli, E. V. Chulkov, P. M. Echenique, and E. Tosatti, Phys. Rev. Lett. **91**, 166803 (2003).
[8] R. A. Bartynski, E. Jensen, T. Gustafsson, and E. W. Plummer, Phys. Rev. B **32**, 1921 (1985).
[9] U. O. Karlsson, S. A. Flodström, R. Engelhardt, W. Gädeke, and E. E. Koch, Solid State Commun. **49**, 711 (1984).
[10] I. Vobornik, J. Fujii, M. Mulazzi, G. Panaccione, M. Hochstrasser, and G. Rossi, Phys. Rev. B **72**, 165424 (2005).
[11] R. Li, H. Ma, X. Cheng, S. Wang, D. Li, Z. Zhang, Y. Li, and X.-Q. Chen, Phys. Rev. Lett. **117**, 096401 (2016).
[12] E. V. Chulkov, V. M. Silkin, and E. N. Shirykalov, Surf. Sci. **188**, 287 (1987).
[13] B. G. Briner, P. Hofmann, M. Doering, H.-P. Rust, E. W. Plummer, and A. M. Bradshaw, Phys. Rev. B **58**, 13931 (1998).
[14] M. F. Crommie, C. P. Lutz, and D. M. Eigler, Nature (London) **363**, 524 (1993).
[15] P. Avouris, I. W. Lyo, R. E. Walkup, and Y. Hasegawa, J. Vac. Sci. Technol. B **12**, 1447 (1994).
[16] M. F. Crommie, J. Electron Spectrosc. **109**, 1 (2000).
[17] P. T. Sprunger, L. Petersen, E. W. Plummer, E. Lægsgaard, and F. Besenbacher, Science **275**, 1764 (1997).
[18] T. Balasubramanian, E. Jensen, X. L. Wu, and S. L. Hulbert, Phys. Rev. B **57**, R6866 (1998).
[19] V. M. Silkin, T. Balasubramanian, E. V. Chulkov, A. Rubio, and P. M. Echenique, Phys. Rev. B **64**, 085334 (2001).
[20] T. Y. Chien, X. He, S.-K. Mo, M. Hashimoto, Z. Hussain, Z.-X. Shen, and E. W. Plummer, Phys. Rev. B **92**, 075133 (2015).
[21] R. Li, J. Li, L. Wang, J. Liu, H. Ma, H.-F. Song, D. Li, Y. Li, and X.-Q. Chen, Phys. Rev. Lett. **123**, 136802 (2019).
[22] M. Hengsberger, R. Frésard, D. Purdie, P. Segovia, and Y. Baer, Phys. Rev. B **60**, 10796 (1999).
[23] M. Hengsberger, D. Purdie, P. Segovia, M. Garnier, and Y. Baer, Phys. Rev. Lett. **83**, 592 (1999).
[24] P. M. Echenique, R. Berndt, E. V. Chulkov, T. Fauster, A. Goldmann, and U. Höfer, Surf. Sci. Rep. **52**, 219 (2004).
[25] J. Friedlein, J. Harm, P. Lindner, L. Bargsten, M. Bazarnik, S. Krause, and R. Wiesendanger, Rev. Sci. Instrum. **90**, 123705 (2019).
[26] Surface alignment and mechanical polishing of the crystals was carried out by Surface Preparation Laboratory (SPL), The Netherlands.
[27] R. Bastasz, Thin Solid Films **121**, 127 (1984).
[28] E. Jensen, R. A. Bartynski, T. Gustafsson, E. W. Plummer, M. Y. Chou, M. L. Cohen, and G. B. Hoflund, Phys. Rev. B **30**, 5500 (1984).
[29] J. Tersoff and D. R. Hamann, Phys. Rev. Lett. **50**, 1998 (1983).
[30] J. Kliewer, R. Berndt, E. V. Chulkov, V. M. Silkin, P. M. Echenique, and S. Crampin, Science **288**, 1399 (2000).
[31] J. Kröger, L. Limot, H. Jensen, R. Berndt, S. Crampin, and E. Pehlke, Prog. Surf. Sci. **80**, 26 (2005).
[32] J. Li, W.-D. Schneider, R. Berndt, O. R. Bryant, and S. Crampin, Phys. Rev. Lett. **81**, 4464 (1998).
[33] K. Schouteden, P. Lievens, and C. Van Haesendonck, Phys. Rev. B **79**, 195409 (2009).
[34] K. B. Ray, X. Pan, and E. W. Plummer, Surf. Sci. **285**, 66 (1993).
[35] G. M. Watson, P. A. Bruhwiler, E. W. Plummer, H.-J. Sagner, and K.-H. Frank, Phys. Rev. Lett. **65**, 468 (1990).
[36] R. Wiesendanger, *Scanning Probe Microscopy and Spectroscopy: Methods and Applications* (Cambridge University Press, Cambridge/New York, 1994).
[37] X.-Y. Hou, F. Zhang, X.-H. Tu, Y.-D. Gu, M.-D. Zhang, J. Gong, Y.-B. Tu, B.-T. Wang, W.-G. Lv, H.-M. Weng, Z.-A. Ren, G.-F. Chen, X.-D. Zhu, N. Hao, and L. Shan, Phys. Rev. Lett. **124**, 106403 (2020).
[38] I. Y. Sklyadneva, E. V. Chulkov, P. M. Echenique, and A. Eiguren, Surf. Sci. **600**, 3792 (2006).
[39] Y. Zhang, V. W. Brar, F. Wang, C. Girit, Y. Yayon, M. Panlasigui, A. Zettl, and M. F. Crommie, Nat. Phys. **4**, 627 (2008).
[40] V. W. Brar, S. Wickenburg, M. Panlasigui, C.-H. Park, T. O. Wehling, Y. Zhang, R. Decker, C. Girit, A. V. Balatsky, S. G. Louie, A. Zettl, and M. F. Crommie, Phys. Rev. Lett. **104**, 036805 (2010).
[41] S.-J. Tang, J. Shi, B. Wu, P. T. Sprunger, W. L. Yang, V. Brouet, X. J. Zhou, Z. Hussain, Z.-X. Shen, Z. Zhang, and E. W. Plummer, Phys. Status Solidi B **241**, 2345 (2004).

[42] M. Schackert, T. Märkl, J. Jandke, M. Hölzer, S. Ostanin, E. K. U. Gross, A. Ernst, and W. Wulfhekel, Phys. Rev. Lett. **114**, 047002 (2015).
[43] J. Jandke, P. Hlobil, M. Schackert, W. Wulfhekel, and J. Schmalian, Phys. Rev. B **93**, 060505(R) (2016).
[44] L. Bürgi, O. Jeandupeux, H. Brune, and K. Kern, Phys. Rev. Lett. **82**, 4516 (1999).
[45] S. Grothe, S. Johnston, Shun Chi, P. Dosanjh, S. A. Burke, and Y. Pennec, Phys. Rev. Lett. **111**, 246804 (2013).
[46] P. T. Sprunger, E. Lægsgaard, and F. Besenbacher, Phys. Rev. B **54**, 8163 (1996).
[47] J. Homoth, M. Wenderoth, K. J. Engel, T. Druga, S. Loth, and R. G. Ulbrich, Phys. Rev. B **76**, 193407 (2007).
[48] J. A. Støvneng and P. Lipavský, Phys. Rev. B **42**, 9214 (1990).
[49] C. Friesen, H. Osterhage, J. Friedlein, A. Schlenhoff, R. Wiesendanger, and S. Krause, J. Phys. D: Appl. Phys. **51**, 324001 (2018).